AM-FM and Loss Tangent Imaging – Two New High Speed and High Resolution Tools for Measuring Quantitative Nanomechanical Properties

Roger Proksch, Irène Revenko, Sophia Hohlbauch, Jason Cleveland, Deron Walters, Nicholas A. Geisse, Amir Moshar, Jason Bemis and Clint Callahan, Asylum Research, Santa Barbara, CA

1 ABSTRACT

Amplitude-modulated (AM) Atomic Force Microscopy (AFM), also known as tapping mode, or AC mode is a proven, reliable and gentle imaging method with widespread applications. Previously, the contrast in AM-AFM has been difficult to quantify. In this work, we introduce two new techniques that allow unambiguous interpretation of material properties. The imaging mode presented here combines the features and benefits of normal AM mode with quantitative and high sensitivity of frequency modulated (FM) mode. Briefly, in AM-FM imaging, the topographic feedback operates in AM mode while the second resonant mode drive frequency is adjusted to keep the phase at 90 degrees, on resonance. With this approach, frequency feedback on the second resonant mode and topographic feedback on the first are decoupled, allowing much more stable, robust operation. The FM image returns a quantitative value of the frequency shift that in turn depends on the sample stiffness and can be applied to a variety of physical models. Loss tangent imaging is a recently introduced quantitative technique that recasts the interpretation of phase imaging in AM mode into one term that includes both the dissipated and stored energy of the interaction between the tip and the sample. Quantifying the loss tangent depends solely on the measurement of cantilever parameters at a reference position.

Keywords: viscoelasticity, nanomechanics, tapping mode, AM mode

2 INTRODUCTION AND MOTIVATION

The macroscopic properties of polymer materials – especially composites – depend on their nanoscale properties. Here we discuss two recently developed techniques for nanoscale properties mapping – Loss Tangent and AM-FM imaging. These measurements are made simultaneously during AM mode[1],[2] imaging and provide quantitative images of the tip-sample loss tangent and of the tip-sample stiffness. With appropriate modeling, this stiffness can be simply converted into an elasticity map.

3 BIMODAL IMAGING

The cantilever is driven at first two flexural resonances in a manner similar to that described earlier.[3] The data shown here was acquired with an MFP-3D or Cypher AFM,[4] using Olympus AC160 cantilevers unless otherwise noted. The response of the cantilever at the two resonances is measured and used in different ways as indicated Figure 1.

1st Resonance: As with AM mode imaging, the first resonance amplitude signal is used in a feedback loop to control the tip-sample separation. The resulting signal from this is used to create a topographic image. At the same time, resulting amplitude and phase information is used to calculate the tip-sample loss tangent.[5]

2nd Resonance: The second mode phase is used in a feedback loop to keep it at resonance. This resonance frequency is related to the tip-sample stiffness and dissipation.[6,7,8]

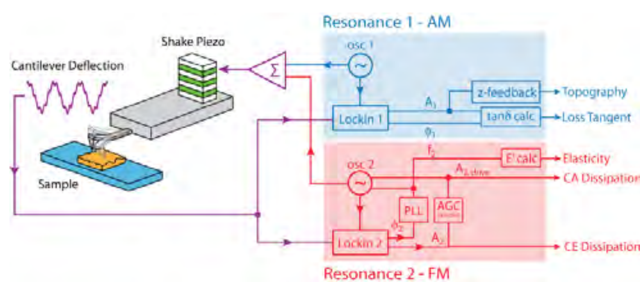

Figure 1: Dual AC™ AM-FM mode. The first mode (blue) controls the tip-sample separation in AM mode yielding the topography and loss tangent image. The second mode (red) is operated in FM mode and reports the tip-sample stiffness and dissipation.

Conventional single mode FM imaging requires relatively complicated feedback schemes where the tip sample spacing is servoed using the cantilever resonance frequency. This is in turn typically tracked using a phase-locked loop (PLL) that keeps the phase at 90 degrees by adjusting the frequency. Finally, another feedback loop is sometimes implemented to maintain the amplitude at a constant value, automatic gain control (AGC). If the AGC is implemented, output amplitude is constant (CA). Otherwise, if the amplitude is allowed to vary, it is termed constant excitation (CE) mode. In either case, the varying response or drive amplitude contains information on the tip-sample dissipation while the frequency f_2 is proportional to the conservative interactions. Simultaneously optimizing three feedback loops can lead to considerable complexity in operating the microscope.[9] In the approach here, the topographic feedback is confined to the first resonant mode

which means much greater stability. For example, if the PLL or AGC control loops operating on the second mode become unstable and oscillate, it has little or no effect on the ability of the first mode to stably track the surface topography.

3.1 First Resonance – Topography and Loss Tangent

The amplitude of the first resonant mode is used to maintain the tip-sample distance. The control voltage, typically applied to a z-actuator results in a topographic image of the sample surface. At the same time, the phase of the first mode will vary in response to the tip-sample interaction. This phase reflects both dissipative[10] and conservative[11] interactions. A tip indenting a surface will both store elastic energy and dissipate viscous energy – the two are inextricably linked. The loss tangent,[12] is a dimensionless parameter measures the ratio of energy dissipated to energy stored in one cycle of a periodic deformation, and is ubiquitous in the polymer literature,[13] [,14,15] An additional attractive feature of the loss tangent of linear viscoelastic materials is independence of the indenter tip contact area.[16, 17, 18] The loss tangent of the tip-sample interaction can be described by the following relation involving the measured cantilever amplitude A_1 and phase φ_1:

$$\tan\delta = \frac{G''}{G'} = \frac{\langle F_{ts}\cdot\dot{z}\rangle}{\omega\langle F_{ts}\cdot z\rangle} = \frac{A_1/A_{1,f} - \sin\varphi}{\cos\varphi}\ . \tag{1}$$

In this expression, F_{ts} is the tip-sample interaction force, z is the tip motion, $\dot{z}$ is the tip velocity, ω is the angular frequency at which the cantilever is driven and $\langle\ \rangle$ represents a time-average. The parameter $A_{1,f}$ is the "free" resonant amplitude of the first mode, measured at a reference position and represents There are a couple of important things to note in Equation (1):

1. Since it only involves the phase and ratios of amplitudes, it does not depend on measurements of the optical lever sensitivity, a large source of error in force-distance curves.[19]
2. Because the denominator of Equation (1) involves the contributions from both attractive and repulsive interactions, represents an lower estimate of the repulsive power. This in turn means that the loss tangent calculated using Equation (1) is a upper limit.

3.2 Second Resonance – Stiffness and Dissipation

Frequency Modulation Atomic Force Microscopy[20] has become a powerful technique for imaging surfaces at atomic resolution,[21, 22, 23] and manipulating atomic surfaces.[24] By measuring the frequency shift as the tip interacts with the surface, it is possible to quantify tip-sample interactions.[25, 26, 27, 28, 29] In particular, the frequency shift of a cantilever in FM mode is given by[30]

$$\Delta f_2 = f_{0,2}\frac{\langle F_{ts} z\rangle}{k_2 A_2^2} \approx \frac{f_{0,2}}{2}\frac{k_{ts}}{k_2}\ . \tag{2}$$

In addition to the terms described for Equation (1) above, $f_{0,2}$ is the second resonance frequency measured at a "free" or reference position, Δf_2 is the shift of the second resonant mode as the tip interacts with the surface, k_2 is the stiffness of the second mode and A_2 is the amplitude of the second mode as it interacts with the surface. As with the expression for the loss tangent, Equation (2) does not directly involve the optical lever sensitivity.

3.3 Simultaneous Loss Tangent and Stiffness Measurements

Since loss tangent can be measured using the first mode and FM is measured using the second resonance mode, both measurements can be made simultaneously. There are some practical experimental conditions to consider when applying this technique to nanomechanical materials properties measurements:

The tip is sensitive to E' and E'' only in repulsive mode. Repulsive mode is favored for:

1. larger cantilever amplitudes (>10nm)
2. stiffer cantilevers (>10N/m)
3. sharp tips and
4. lower setpoints (typically 50% of the free amplitude in this paper).

As a check, the first mode phase should always be <90° and typically <50° for the majority of materials. This assures you are sampling the repulsive tip-sample interactions. Good feedback tracking (avoid parachuting, make sure trace and retrace match) assures good sampling of the mechanical properties. Finally, the accuracy of both techniques depends strongly on careful tuning of the cantilever resonances. Specifically, the resonances should be <10Hz error and the phase should be within 0.5 degrees. These are more stringent conditions than usual for AM mode but are well within the capabilities of the AFMs used here.

Figure 2 below shows an example of simultaneous loss tangent and stiffness mapping of a elastomer-epoxy sandwich. A natural rubber sheet was bonded to a latex

rubber sheet with an epoxy. The sandwich was then microcryotomed and imaged. From macroscopic measurements, the elasticity E ~ 40MPa (natural rubber):4GPa (epoxy):43MPa (latext rubber) measured with a Shore durometer, while the macroscopic loss tangents were estimated to be 1.5, 0.1:2 and 2, respectively, measured with a simple drop test. An AC160 cantilever with a fundamental resonance of 310kHz and a second mode resonance of 1.75MHz was used.

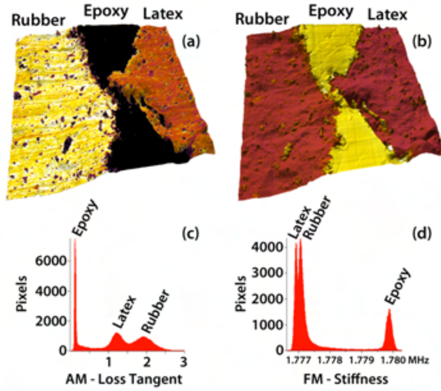

Figure 2: (a) AM – Loss Tangent and (b) FM – Stiffness maps acquired with the first and second resonance respectively. (c) the Loss Tangent histogram and (d) Stiffness histograms. As expected from the bulk data, the loss tangents of the rubber and latex are larger than the epoxy and clearly separated from each other (~1.5 for latex and ~2 for the natural rubber) in the Loss Tangent histogram (c). The bulk moduli for the latex and rubber are quite close, ~40MPa and 43MPa respectively. Despite being so close, the two materials are clearly separated in the Stiffness histogram (d). Note that the surface roughness was on the order of 500nm.

Figure 3 below shows an example of a very smooth sample – graphene on SiO2. The graphene layeres showed very different stiffness and loss tangent than the substrate despite being extremely thin.

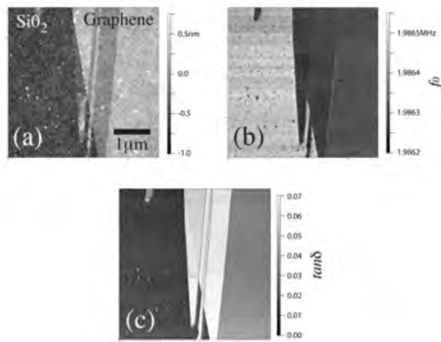

Figure 3. Graphene on SiO2. (a) topography, (b) AM-FM and (c) loss tangent images of a graphene on SiO_2. Note that the graphene appears less stiff than the substrate. The edge layers exhibit a larger loss tangent, indicative perhaps of humidity trapped between the graphene and SiO_2.

3.4 Elasticity Mapping

Since the second mode resonance depends on the interaction stiffness k_{ts}, the material modulus can be mapped by applying a particular mechanical model. One of the most simple models is a Hertz indenter in the shape of a punch. In this case, the elasticity of the sample is related to the tip-sample stiffness by the relation $k_{ts} = 2E'a$, where a is a constant contact area. Combining this with equation (2) above results in the expression

$$E' = \frac{\Delta f_2}{f_{0,2}} \frac{k_2}{a} . \tag{3}$$

Thus if the contact area and spring constant are known, the sample modulus can be calculated. Of course, other tip shapes could be used in the model. Calibration of the tip shape is a well-known problem, beyond the scope of this paper. However, it is possible to use a calibration sample that circumvents this process. As a first step, we have used a NIST-traceable ultra high molecular weight high density polyethelene (UHMWPE)[31] sample to first calibrate the response of the AC160 cantilever. Equation (3) can be rewritten as $E' = C_2 \Delta f_2$, where C_2 is a constant, measured over the UHMWPE reference that relates the frequency shift to the elastic modulus. This can then be applied to unknown samples. An example is shown in Figure 4, where the elasticity of a cryo-microtomed spectra fiber embedded in epoxy is shown.

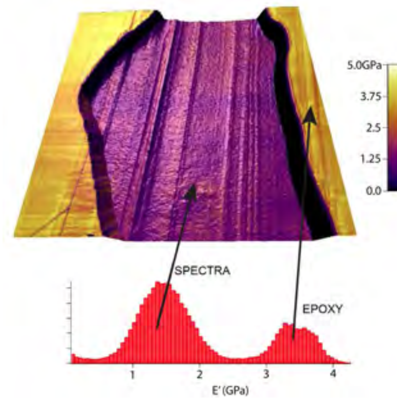

Figure 4. Elastic modulus of Spectra Ultra-high Molecular Weight Polyethelene fibers (Honeywell) embedded in epoxy. The elastic modulus calculated using Equation (3) rendered on a topographic image. 5um scan. Sample courtesy of Dr. Ken Strawhecker, U.S. Army Research Lab.

3.5 High Speed Elasticity Mapping

Finally, this technique can be performed at high speeds using small cantilevers. The response bandwidth of the ith

resonant mode of a cantilever is $BW_i = f_{i,0}/\pi Q_i$ where $f_{i,0}$ is the resonant frequency of the ith mode and Q_i is the quality factor. To increase the resonance frequency without changing the spring constant can be done by making cantilevers smaller.[32] In contrast to normal AM imaging, the second resonant mode must still be accessible to the photodetector, requiring $f_{2,0} < 10MHz$ for the Cypher AFM. An example is shown in Figure 5, where a EPDH/Epoxy cryo-microtomed boundary is measured at a 2Hz and 20Hz line scan rates. These images were acquired with an AC55 cantilever from Olympus ($f_{1,0} \approx 1.3MHz, f_{120} \approx 5.3MHz$).

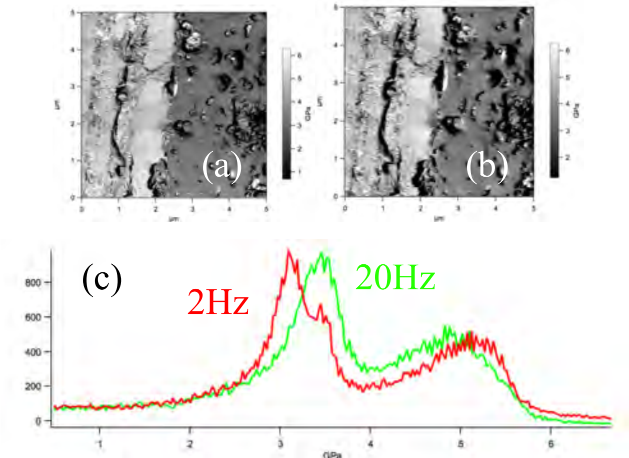

Figure 5 Elasticity images of Epoxy/EPDH bond imaged at 2Hz (a) and at 20Hz (b) line scan rates with an Olympus AC55 cantilever. (c) the elasticity histogram. 5μm scan.

4 CONCLUSIONS

Loss tangent and AM-FM provide two additional tools for quantifying nanoscale mechanical properties. These modes are compatible with conventional AM imaging, meaning that high resolution, high speed mechanical properties can be made on an enormous variety of samples.

5 REFERENCES

[1] G. Binng, C. Quate and C. Gerber, Phys. Rev. Lett., **56**, 930 (1986).

[2] P. Gleyzes, P. K. Kuo, and A. Boccara, Appl. Phys. Lett., **58**, 2989 (1991).

[3] R. Proksch and D. Yablon, Appl. Phys. Lett., **100**, 073106 (2012).

[4] www.AsylumResearch.com

[5] R. Proksch, D. Yablon, and A. Tsou, ACS Rubber Division 180th Technical Meeting, 2011-24 (2011).

[6] US Patents 8,024,963, 7,937,991, 7,603,891, 7,921,466 and 7,958,563 with others pending.

[7] S. D. Solares and G. Chawla, J. Appl. Phys., **108**, 054901 (2010).

[8] S. Guo, S. D. Solares, V. Mochalin et al., Small **8**, 1264 (2012).

[9] J. I. Kilpatrick, A. Gannepalli, J. P. Cleveland and S. P. Jarvis, Rev. Sci. Inst., 80, 023701 (2009).

[10] J.P. Cleveland, B. Anczykowski, A.E. Schmid, V.B. Elings, Appl. Phys. Lett. **72**, 2613-2615 (1998).

[11] A. San Paulo and R. Garcia, Physical Review B **66** (4), 041406 (2002).

[12] J. D. Ferry, *Viscoelastic properties of polymers*, 3rd ed. (John Wiley and Sons, New York, 1980).

[13] C. G. Robertson and M. Rackaitis, Macromolecules **ACS ASAP** (2011).

[14] R. Mohr, K. Kratz, T. Weigel, M. Lucka-Gabor, M. Moneke and A. Lendlein, Proceedings of the National Academy of Sciences **103** (10), 3540-3545 (2006).

[15] E. Munch, J. Pelletier, B. Sixou, G. Vigier, Physical Review Letters **97**, 207801 (2006).

[16] P. C. Painter and M. M. Coleman, *Essentials of Polymer Science and Engineering*. (DEStech Publications Inc., Lancaster, 2009).

[17] Y. Cao, X. Ji, and X. Feng, Philosophical Magazine **90** (12), 17 (2010).

[18] C. A. Tweedie, G. Constantinides, K. E. Lehman, D.J. Brill, G.W. Blackman, K.J. Van Vliet., Advanced Materials **19**, 2540 (2007).

[19] R. Wagner, R. Moon, J. Pratt, G. Shaw and A. Raman Nanotechnology **22** 455703 (2011).

[20] T. R. Albrecht, P. Grütter, D. Horne, and D. Rugar, J. Appl. Phys. **69**, 668 (1991).

[21] N*oncontact Atomic Force Microscopy*, edited by S. Morita, R. Wiesendanger, and E. Meyer, Springer, Berlin, (2002).

[22] F. J. Giessibl, Rev. Mod. Phys. **75**, 949 (2003).

[23] R. García and R. Pérez, Surf. Sci. Rep. **47**, 197 (2002).

[24] Y. Sugimoto, M. Abe, S. Hirayama, N. Oyabu, O. Custance, and S. Morita, Nat. Mater. **4**, 156 (2005).

[25] M. A. Lantz, H. J. Hug, R. Hoffman, P. J. A. van Schendel, P. Kappenberger, S. Martin, A. Baratoff, and H. J. Guntherodt, Science **291**,2580 (2001).

[26] N. Oyabu, P. Pou, Y. Sugimoto, P. Jelinek, M. Abe, S. Morita, R. Pérez, and O. Custance, Phys. Rev. Lett. **96**, 106101 (2006).

[27] Y. Sugimoto, P. Pou, O. Custance, P. Jelinek, S. Morita, R. Perez, and M. Abe, Phys. Rev. B **73**, 205329 (2005).

[28] Y. Sugimoto, P. Jelinek, P. Pou, M. Abe, S. Morita, R. Perez, and O.Custance, Phys. Rev. Lett. **98**, 106104 (2007).

[29] Y. Sugimoto, P. Pou, M. Abe, P. Jelinek, R. Perez, S. Morita, and O. Custance, Nature(London) **446**, 64 (2007).

[30] F. J. Giessibl, Phys. Rev. B **56**(24) 16010 (1997).

[31] NIST Ultra High Molecular Weight Polyethelene, reference material 8456.

[32] D. A. Walters, J. P. Cleveland, N. H. Thomson et al. Rev. Sci. Inst., **67** 3583 (1996).